Sciencia Acta Xaveriana
An International Science Journal
ISSN. 0976-1152

Volume 3
No. 1
pp. 27-44
Apr 2012

Growth and characterization of 4-N, N-dimethylamino-4'N'-methylstilbazolium p-toluenesulphonate (DAST) crystal- A potential THz emitter

R. Gunaseelan[1], A. Antony Raj[1], S. Selvakumar[2] and P. Sagayaraj[1*]

[1] Dept.of Physics, Loyola College, Chennai- 600034, India

[2] Department of Physics, Nandanam Govt. Arts College, Chennai- 600 039, India

[1*] Associate professor of Physics, Loyola College, Chennai - 600 034, India
Email: psagayaraj@hotmail.com, Tel: +9144 28178200; Fax: +9144 28175566

Abstract : We have adopted slope nucleation coupled slow evaporation method for the growth of high quality 4-N, N-dimethylamino-4-N-methyl-stilbazoliumtosylate (DAST) crystals. The structure of the crystal was studied by single crystal X-ray diffraction analyses. The FTIR results reveal the existence of the vinyl groups and their corresponding vibrational modes. The linear and nonlinear optical properties are studied by UV-Vis absorption and SHG test. The melting point and thermal behavior of DAST were investigated using differential scanning calorimetric (DSC) and thermogravimetric(TG) analyses (TGA). The electrical properties of the crystal are investigated by dielectric and photoconductivity measurements.

Key words: Terahertz; Solution Growth; Organic crystal; NLO; Single crystal XRD; Thermal stability.

1. Introduction

For high-speed second-order nonlinear optical (SONLO) applications, such as electro-optics (EO), second-harmonic generation (SHG), optical parametric oscillation (OPO), and optical rectification (OR), including terahertz (THz) wave generation, a highly asymmetric electronic response of the material to the external electric field is required [1]. In electricfield sensors, the commonly used inorganic EO crystals are $LiTaO_3$ and $KTiOPO_4$ (KTP) for transverse-field probing and CdTe and ZnTe for longitudinal probing. However, the performance of these sensors has reached its limits. Therefore, high-performance EO materials are required to achieve a higher sensitivity and a wider frequency range. Recently, organic NLO crystals have attracted considerable interest because of their large EO coefficient and small dielectric constant [2].

Among the various classes of materials investigated worldwide, ionic organic crystals are of special interest due to their advantageous mechanical, chemical and thermal properties [3, 4]. One of the most successful approaches to develop highly polar organic NLO crystals is based on using strong Coulomb interactions to achieve noncentrosymmetric crystalline packing. The most well-known and widely investigated ionic crystal in this family is; 4-N, N-dimethylamino-4-N-methyl-stilbazoliumtosylate (DAST). DAST was first reported in 1989 by Marder et al and is still being recognized as the state-of the-art organic NLO crystal [5].

DAST is an organic salt that consists of a positively charged stilbazolium cation and a negatively charged tosylate anion. The molecular structure of the cation in DAST consists of two aryl rings adopting the expected trans arrangement about the ethylenic linkage. In crystalline DAST, the deviation of the molecules from a completely aligned system is the 20^0 angle between the long axis of the cations and the polar *a*-axis of the crystal. The arrangement of alternating cationic and anionic sheets can facilitate the formation of macroscopically polar structures [6].

Though the DAST crystal is the best organic THz emitter ever studied, the growth of high optical quality DAST single crystal is still a challenge, one of the challenges is to reduce the growth time needed to obtain high optical quality DAST, which takes several weeks for crystals with dimensions exceeding 1 cm^3 [7]. Faster and easier crystal growth procedure is an important challenge for future applications and therefore optimization of the growth techniques and the development of new molecules for crystal growth are subjects of present research. Different approaches

have been adopted to achieve faster and improved growth rate of DAST crystals. The difficulties in growth positioning and nucleation are effectively solved by combining the slope nucleation method (SNM) with the laser irradiation method (LIM) [8]. A cost effective method has been suggested by Brahadeeswaran et al by using solutions of lower super saturation coupled with isothermal solvent evaporation and this method facilitated the development of nearly parallel (001) and ($00\bar{1}$) faces so as to directly utilize the crystals for EO and THz applications [9].

Nagaoka et al compared the EO sensitivity of DAST crystal with KTP crystal and found that the EO sensitivity of the DAST was more than 30-fold than that of the KTP [2]. Waveguiding has been demonstrated in DAST channel waveguides and Mach-Zehnder modulators are structured by using 30 keV e-beam irradiation and the result gives a new perspective for the use of nonlinear optical organic materials for integrated optics [10]. Minamide et al have achieved high-sensitivity, rapid response detection of THz waves using DAST [11]. Both the generation and detection of THz waves via DAST crystals were realised, which may open the door to new THz wave applications. Similarly, ultrabroadband (1.5–37 THz) THz wave generation using DFG in DAST crystal was demonstrated by Ito et al [12].

For many photonic applications, a thin crystal or thin film is more attractive. The experiments conducted by Han et al proved that DAST crystals with a thickness of a few hundred micrometers are suitable for EO sampling up to few THz [13]. It has been reported that the as-grown and very thin crystals are less sensitive to thermal shock when compared to thick DAST crystals due to large thermal gradients and these thin DAST crystals are preferable to avoid defects [14]. Inspired with these facts, we have made an attempt to investigate the growth of DAST crystals by slightly modifying the slope nucleation method and obtained reasonably good quality thin plates of DAST crystals. We have characterized the grown DAST crystals employing the single crystal XRD, FTIR, linear and nonlinear properties, dielectric and photoconductivity studies.

2. Experimental

2.1 Synthesis

DAST was prepared by metathesization of the N,N-dimethylamino-N'-methylstilbazolium iodide (DMSI) salt with sodium p-toluenesulfonate. DMSI (cation) was synthesized by the

condensation of 1, 4-dimethyl pyridinium iodide (2.35 g, 10 mmol), methanol (30 ml) and 4-N, N-dimethylamino-benzaldehyde (1.79 g, 10 mmol) in the presence of piperidine (0.2 ml) [15]. The above mixture was refluxed for 20 hours and then cooled to room temperature. The product was filtered and recrystallized from methanol for nearly 5 times. Sodium p-toluenesulfonate was synthesized as follows; p-toluenesulfonate (1.588 g, 0.01 mol) was taken in a 100 ml capacity beaker and 50 ml of Millipore water was added, it was then stirred and heated at 60° C for 1 hour. In another 100 ml capacity beaker, 30 ml of Millipore water was taken to which NaOH (0.4 g, 0.01 mol) was added, and it was stirred and heated at 70° C for 1 hour. Later, these two hot solutions were mixed thoroughly which yielded a white precipitate. The precipitate was collected and then completely dried in an electric furnace at 100° C for 5 hrs.

In the next stage, the metathesizaton reaction was carried out. Initially, 0.732 g (2 mmol) of DMSI was dissolved in 100 ml of distilled water by heating and simultaneously 0.4292 g (2 mmol) of sodium p-toluenesulfonate was dissolved in 30 ml of water with continued heating. These two hot solutions were mixed and further heated for 30 minutes at 70° C and then cooled to room temperature. The reaction resulted in the appearance of a red precipitate and the left out aqueous sodium iodide was separated from the former by vacuum filtration. The purity of DAST was further improved by successive recrystallization.

2.2 Solubility

The recrystallized synthesized salt of DAST was used to measure the solubility in methanol. A 250 ml capacity glass beaker containing 100 ml of methanol was placed in the temperature bath. Initially the temperature was set as 30^{o}C, the beaker was closed with an acrylic sheet containing a hole at the center through which the stirrer was dipped into the solution. Both the addition of powdered sample of DAST to the solution in small amounts and subsequent stirring of the solution by a motorized stirrer were continued till the excess salt was deposited at the bottom of the beaker. The stirring was further continued, to ensure homogeneous temperature and concentration throughout the entire volume of the solution. After confirming the saturation, the content of the solution was analyzed gravimetrically. A 20 ml of the saturated solution of the sample was withdrawn by means of a warmed pipette and the same was poured into a cleaned, dried and weighed petri dish. The solution was then kept for slow evaporation in a heating

mantle till the solvent was completely evaporated. The mass of DAST in 20 ml of solution was determined by weighing the petri dish with salt and hence the solubility ie., the quantity of DAST salt (in gram) dissolved in 100 ml of methanol was determined. The solubility of DAST salts in methanol was determined for five different temperatures (30, 35, 40, 45 and 50 °C) by adopting the above procedure and the solubility curve is shown in Fig. 1.

2.3 Crystal Growth

Crystal growth was performed by employing slope nucleation method coupled with slow evaporation technique. A saturated solution was prepared with 3.25 g of DAST dissolved in 100 ml of methanol at 40 °C and then stirred for 1 hr. The beaker was sealed with a perforated lid and the solvent was allowed to evaporate slowly. As glass beakers produced only very poor needle crystals due to multi-nucleation, Teflon beaker was used in order to prevent the sticking of material to the side walls of the beaker during evaporation process. After 6 days, crystals size of 11 x 4 x 3 mm^3 was obtained (Fig. 2).

3. Results and Discussion

3.1 Single crystal X-ray Diffraction analysis

The grown crystal was subjected to single crystal X-ray diffraction studies using Bruker Kappa APEXII single crystal X-ray diffractometer with MoK_α radiation ($\lambda = 0.7170$ Å) to solve the structure. The calculated lattice parameters of grown DAST crystals are presented in Table 1. The XRD data indicates that the crystal are identical with *monoclinic* structure and belong to noncentrosymmetric space group Cc. The XRD data almost fits well with the earlier work [16].

3.2 FT-IR analysis

Vibrational spectroscopy has been extensively used to understand the factors contributing to the linear electro-optic (LEO) effect from the Vibrational modes in organic materials and to provide deeper knowledge regarding the intermolecular interactions and the relationship between molecular architecture, nonlinear response and hyperpolarizability [17]. The vibrational spectral analysis of DAST is performed on the basis of the characteristic vibrations of the stilbazolium cation and toluene sulfonate anion. The stilbazolium cation group comprises the vinyl group L.

vibrations, phenyl ring vibrations and methyl group vibration while the tosylate anion group encompass the sulfonate group and skeletal vibrations.

The FTIR spectrum for DAST crystal was recorded in the wavelength range 400 to 4000 cm^{-1}. In Fig. 3, the peak at 3035.96 cm^{-1} is assigned to the aromatic C-H stretch. The peak at 2914 cm^{-1} is assigned to the alkyl C-H stretch. The alkene bond stretching vibrations in conjugated systems without a centre of symmetry interact to produce two C=C stretching bands, near 1650 and 1600 cm^{-1}. The peaks at 1584.32 and 1527.63 cm^{-1} are attributed to the aromatic ring vibrations. The peak at 1369.87 cm^{-1}corresponds to CH_2 bending and C-N stretching mode. The peak at 825.51 cm^{-1} is assigned to the 1, 4 distributed aromatic ring. The in-plane and out-plane deformations bands are observed, as expected, in the regions 1510-1000 cm^{-1} and 1000-750 cm^{-1}, respectively. The spectrum further shows that the bands in the range 4000 to 2500 cm^{-1} are relatively less intense, suggesting that the grown crystal is an ordered single crystal in nature [18]. The Vibrational wavenumbers and their tentative assignments are given in Table 2. Most of the assignments presented in this work are in close agreement with the recent work on the spectroscopic analysis of DAST crystal carried out by Vijayakumar et al employing the near infrared Fourier transform (NIR FT) Raman and Fourier transform infrared (FT-IT) spectra [19]. Though several functional groups of anions were investigated corresponding to the stilbazolium cation, the toluene sulfonate (tosylate) anion has been established to be the excellent counterion that helps in enabling the DAST crystal to be efficient electro-optic crystal by providing the noncentosymmetric structure. Therefore, the structural features and vibartional analysis of this functional group are of valuable for spectroscopists.

3.3 Optical absorption spectral analysis

The absorption spectra of the DAST crystal were recorded in solid phase as well as in solution phase (Methanol) are shown in Fig. 4. The absorption spectrum of DAST in methanol shows two distinct absorption peaks; the appearance of this kind of peaks was reported by Kumar et al and Jagannathan and Kalainathan [20, 21]. The minor peak at 275 nm corresponds to the n-π* transition and the major peak with maximum absorption at around 475 nm represents the π-π* transition and the absorption peak λ_{max} value is in agreement with the λ_{max} of 474 nm reported by Marder et al [16].

3.4 NLO test-Kurtz and Perry powder SHG test

DAST crystal is perhaps, one of the most widely studied material for its NLO properties. DAST crystals are of great interest for second order NLO applications, such as frequency conversion and optical parametric oscillation in waveguides. There are hundreds of articles in reputed journals, conference proceedings and books that deal with the NLO and THz properties of DAST crystals. The data on its second harmonic efficiency, effective nonlinear optical co-efficient, phase matching possibilities and electro-optic co-efficient are discussed and reviewed by researchers [5].

The second harmonic generation test was done on the DAST sample using Kurtz and Perry technique [22]. The source used was Q-switched, mode-locked Nd^{3+}:YAG laser emitting 1.06 μm fundamental radiation. The input laser beam was passed through IR reflector and then directed on the microcrystalline powdered sample packed in a capillary tube of diameter 0.154 mm. For the SHG efficiency measurements, microcrystalline material of urea was used for comparison. The data was collected for broad distribution of particle size ranging from 50-140 μm. When a laser input of 6.2 mJ was passed through DAST, second harmonic signal of 532 nm was produced and the experimental data confirmed a SHG efficiency of nearly 240 times that of standard urea.

3.5 Thermal Analysis

The thermal behaviour of DAST grown crystal was investigated by Differential scanning calorimetry (DSC) and thermogravimetric analysis (TGA) using Perkin-Elmer DSC-7 and TGA-7 spectrometers. The TG-DTA thermogram (Fig. 5) represents the thermal behaviour of DAST crystal and it is observed that the decomposition of the sample begins at around 300^0 C and there is no weight loss up to 300^0 C. In the DTA trace, the presence of exothermic peak at around 320^0 C could be attributed to the complete breakage of the stilbazolium ion from DAST. It has been reported that DAST is known to thermally decompose above its melting temperature of 259 °C [23]. Thus the thermal analysis carried out in this work ascertains that DAST is thermally stable up to 260.32° C and free from any form of impurities. The DSC traces (Fig. 6) reveal that the melting endotherm of DAST crystal is 260.32^o C and there is no evidence of crystal-crystal phase transitions at lower temperatures, which is in agreement with earlier report [16].

3.6 Dielectric Studies

Dielectric permittivity measurements were carried out on the (0 0 1) face of the DAST crystals. The sample was silver coated and then placed inside a dielectric cell and the capacitance measurements were done for temperature at 55°C, 75 °C, 95 °C and 115 °C in the frequency range 50 Hz to 5 MHz using HIOKI 3532-50 LCR Hitester. Fig. 7 and Fig. 8show the plot of log dielectric constant ε′ as a function of log frequency and the plot of dielectric loss (D) as a function of log frequency for DAST crystal respectively. It is observed that both dielectric constant and dielectric loss exhibits similar variation with frequency. The graphs show that the dielectric constant and the dielectric loss are both inversely proportional to frequency. This is a normal dielectric behaviour that both ε′ and D decrease with increasing frequency [24]. This can be understood on the basis that the mechanism of polarization is similar to that of conduction process. Further, the dielectric constant value of DAST sample is found to increase with increasing temperature. In DAST, as temperature increases it normally becomes more ionic in nature.

3.7 Photoconductivity studies

Fig. 9 and show the variations of both photocurrent and dark current with applied field for DAST crystal. In the present study, it is observed that the photocurrent is higher than the dark current at all the applied field values, hence it can be concluded that DAST exhibits positive photoconductivity. This phenomenon can be attributed to the generation of mobile charge carriers caused by the absorption of photons [25]. The photo response of the rapidly grown as well as slow evaporation grown DAST crystals is almost similar. The present study indicates that the photocurrent is almost 8-9 times that of the dark current for a given applied field. This observation is in agreement with the photoconductivity measurements conducted by Follonier et al [26].

4. Conclusion

Single crystal of DAST has been successfully grown by slope nucleation coupled with slow evaporation method. XRD study confirms that DAST belongs to the *monoclinic* crystal system with *Cc* space group. The structural features and vibrational functional group of DAST were assigned from FTIR analysis. The SHG property was tested by using Nd:YAG laser. The 10.

second harmonic efficiency of DAST crystal is found to be very high when compared to Urea. The dielectric studies prove that the sample has low dielectric constant and dielectric loss values at high frequency.

Acknowledgement

The authors acknowledge the University Grants Commission (UGC), India for funding this research work (Ref. No. F. 38-119/2009(SR)).

5. References

[1] M. Jazbinsek, L. Mutter and P. Gunter, IEEE J. Sel. Top. Quantum Electron. 14 (2008) 1298.

[2] K. Nagaoka, H. Adachi, S. Brahadeeswaran, T. Higo, M. Takagi, M. Yoshimura, Y. Mori, T. Sasaki, Jpn. J. Appl. Phys. 43 (2004) L261.

[3] G.R. Meredith, ACS Symposium series 233, American Chemical Society, Washington, DC. (1983) 27.

[4] B.J. Coe, J.A. Harris, A.K. Clays, G. Oibrechts, A. Persoons, J.T. Hupp, R.C. Johnson, S.J. Coles, M.B. Hursthouse, K. Nakatani, Adv. Funct. Mater. 12 (2002) 110.

[5] S.R. Marder, J.W. Perry and W.P. Schaefer, Science. 245 (1989) 626.

[6] B.J. Coe, J.A. Harris, S.J. Coles, M.B. Hursthouse, Acta Crystallogr. C 57 (2001) 857.

[7] H. Adachi, Y. Takahashi, J. Yabuzaki, Y. Mori and T. Sasaki, J. Crystal Growth, 198/199 (1999) 568.

[8] F. Tsunusada, T. Iwai, T. Watanabe, H. Adachi, M. Yoshimura, Y. Mori and T. Sasaki, J. Crystal Growth 237 (2002) 2104.

[9] S. Brahadeeswaran, S. Onduka, M. Takagi, Y. Takahashi, H. Adachi, T. Kamimura, M. Yoshimura, Y. Mori, K. Yoshida and T. Sasaki, Cryst. Growth Des. 6 (2006) 2463.

[10] Mutter, F.D.J. Brunner, Z. Yang, M. Jazbinsek, P. Gunter, J. Opt. Soc. Am. B 9 (2007) 2556.

[11] H. Minamide, J. Zhang, R. Guo, K. Miyamoto, S. Ohno, H. Ito, Appl. Phys. Lett. 97 (2010) 121106.

[12] H. Ito, K. Suizu, T. Yamashita, A. Nawahara, T. Sato, Jpn. J. Appl. Phys. 46 (2007) 7321.

[13] P.Y. Han, M. Tani, F. Pan and X. C. Zhang, Opt. Lett. 25 (2000) 675.

[14] P. Lavent, C. Medrano, B. Ruiz and P. Gunter, Chimia, 57 (2003) 349.

[15] Z. Yang, S. Aravazhi, A. Schneider, P. Seiler, M. Jazbinsek and P. Gunter, Adv. Funct. Mater. 15 (7) (2005) 1072-1076.

[16] S.R. Marder, J.W. Perry, C.P. Yakymyshyn, Chem. Mater. 6 (1994) 1137.

17] C. Bosshard, R. Spreiter, I. Degiorgi and P. Gunter, Phys. Rev. B, 66 (2002) 205107.

[18] Y.W. Chen-Yang, T.J. Sheu, S.S. Lin and Y.K. Tu, Current. Appl. Phys., 2 (2002) 349-353,.

[19] T. Vijayakumar, H.I. Joe, C.P.R.I. Nair, M. Jazbinsek and V.S. Jayakumar, J. Raman Spect., 40 (2008) 52-63.

[20] K. Kumar, R. Rai and S.B. Rai, Appl.Phy B: Lasers and Optics, 96 (2009) 85-94.

[21] K. Jagannathan and S. Kalainathan, J. Cryst. Growth, 310 (2008) 2043–2049.

[22] S.K. Kurtz and T.T. Perry, J. Appl. Phys. 39 (1968) 3798–38l3.

[23] W. Geis, R. Sinta, W. Mowers, S.J. Deneault, M.F. Merchant, K.E. Krohn, S.J. Spector, D.R. Calawa and T.M. Lyszczarz, Appl. Phys. Lett. 84 (2004) 3729.

[24] J.C. Anderson, Dielectrics, Chapman and Hall, 1964.

[25] V. N. Joshi, Photoconductivity, Marcel Dekker, New York 1990.

[26] S. Follonier, M. Fierz, I. Biaggio, U. Meier, C. Bosshard, P. Gunter, J. Opt. Soc. Am. B 19 (2002) 1990.

Figure Caption

Fig. 1 Solubility curve for DAST

Fig. 2 Photograph of DAST crystal

Fig. 3 FTIR spectrum of DAST crystals

Fig. 4 Absorption spectrum of DAST

Fig. 5 TG-DTA traces of DAST crystal

Fig. 6 DSC thermogram of DAST crystal

Fig. 7 Frequency dependence of dielectric constant of DAST crystal

Fig. 8 Frequency dependence of dielectric loss of DAST crystal

Fig. 9 Variation of Photo and dark currents with applied electric field for DAST crystal

Table Caption

Table 1 Single XRD data of DAST crystal

Table 2 FTIR wavenumber assignment for DAST crystal

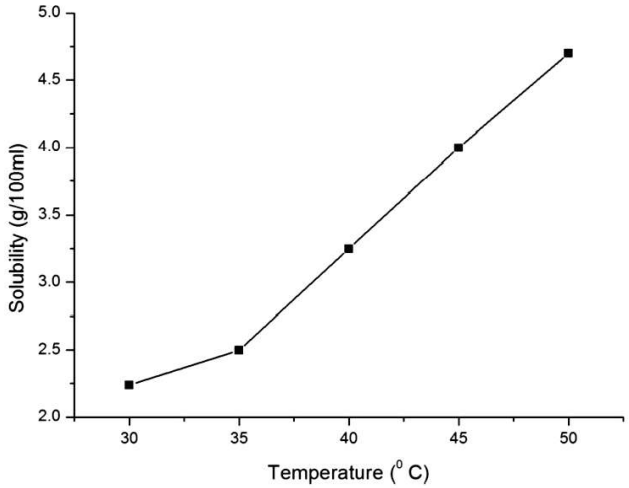

Fig. 1 Solubility curve for DAST

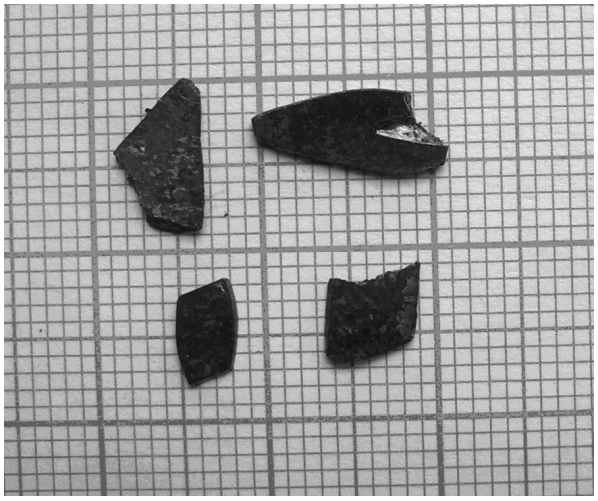

Fig. 2 Photograph of DAST crystals

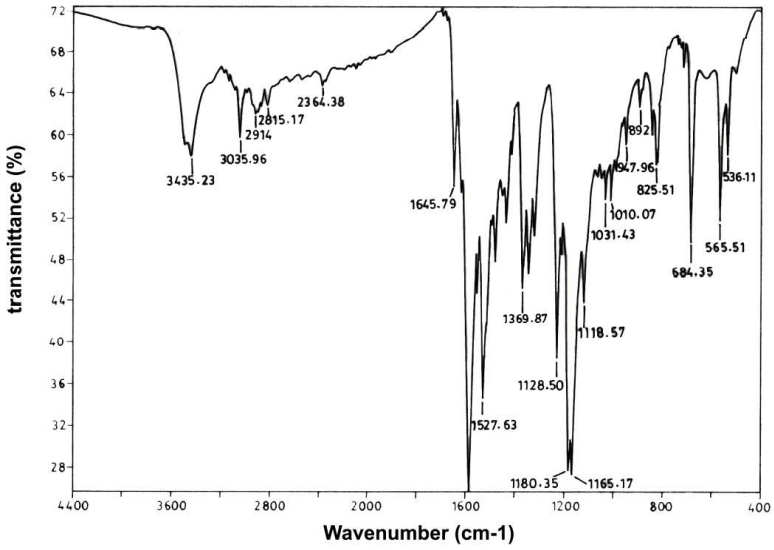

Fig. 3 FTIR spectrum of DAST crystal

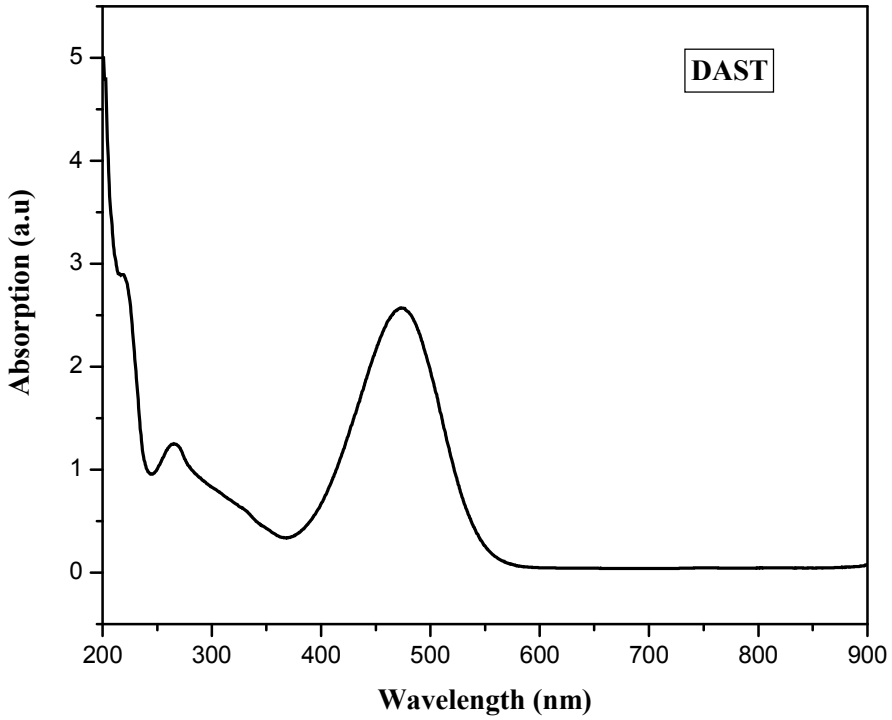

Fig. 4 Absorption spectrum of DAST

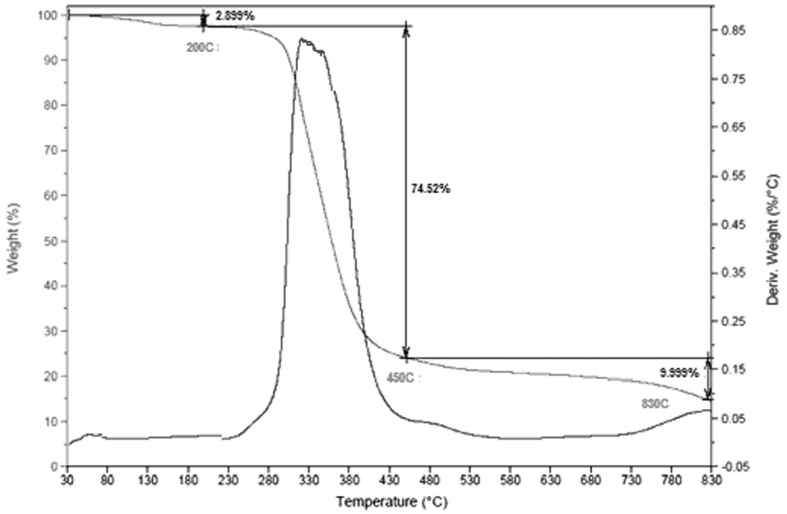

Fig. 5 TG-DTA traces of DAST crystal

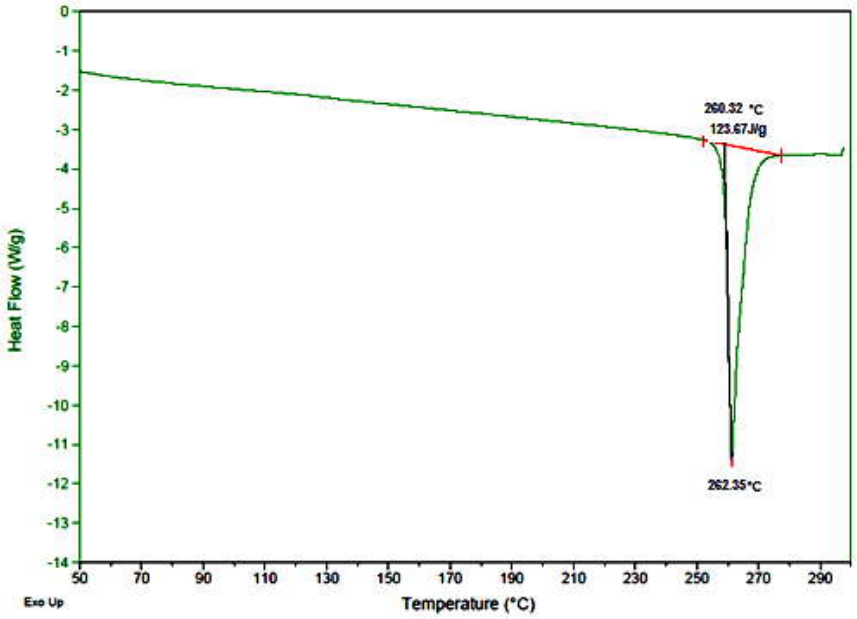

Fig. 6 DSC thermogram of DAST crystal

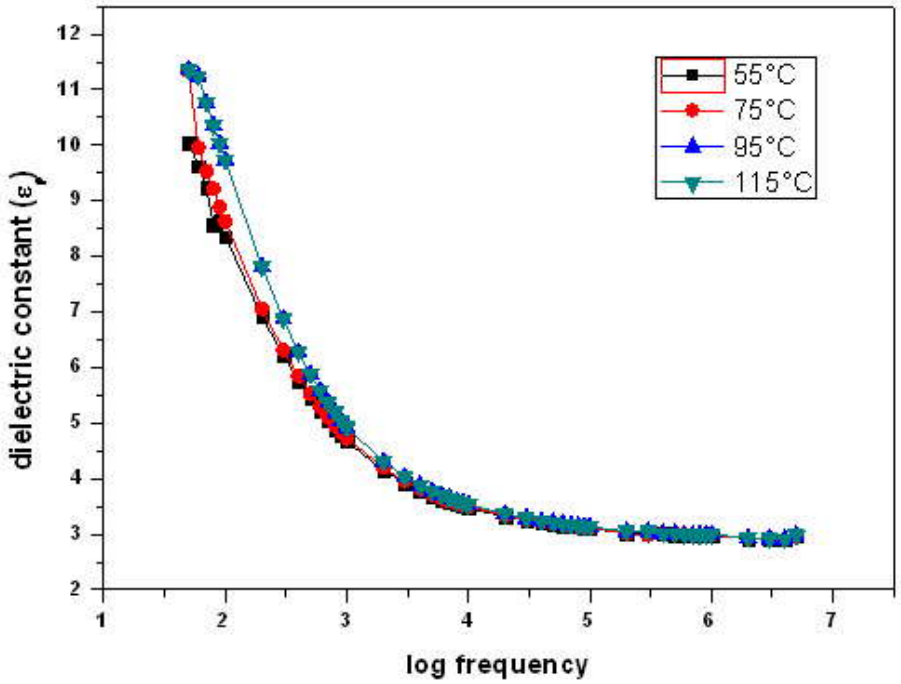

Fig. 7 Frequency dependence of dielectric constant ofDAST crystal

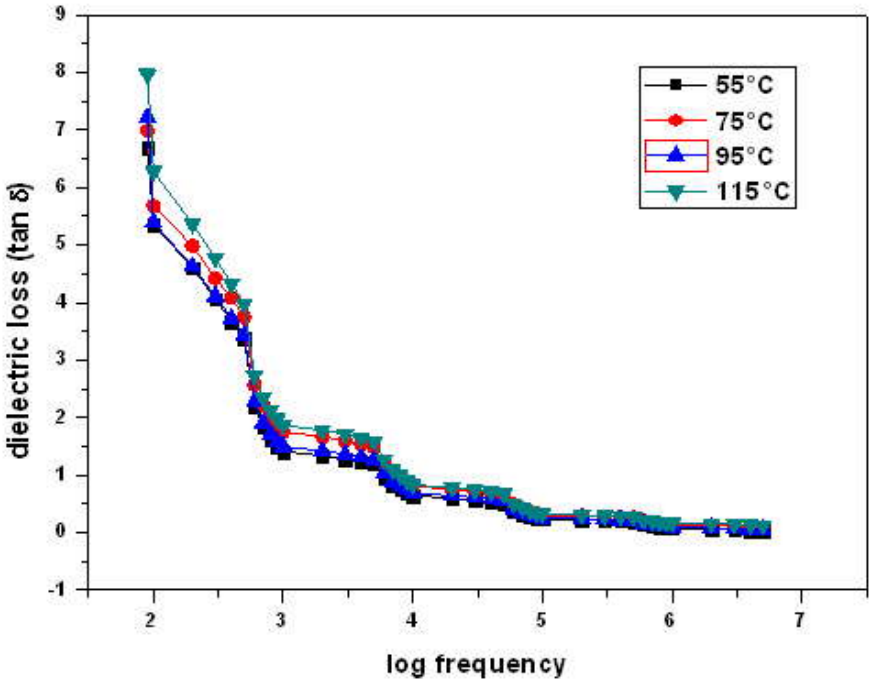

Fig. 8 Frequency dependence of dielectric loss of DAST crystal

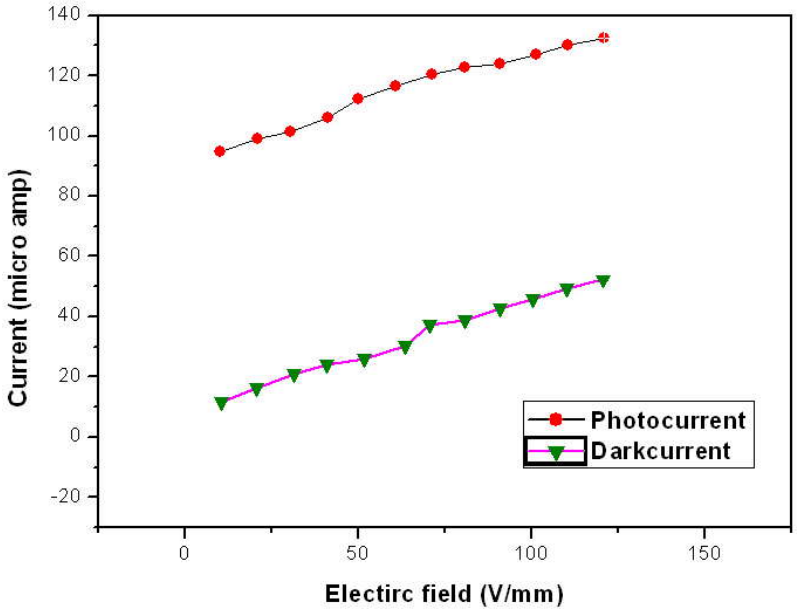

Fig. 9 Variation of Photo and dark currents with applied electric field for DAST crystal

Table 1 Single XRD data of DAST crystal

Compound	DAST Crystal
Formula	$C_{23}H_{26}N_2O_3S$
Formula weight (g/ml)	410.53
Crystal system	Monoclinic
Space group	Cc
a (Å)	10.3652(5)
b (Å)	11.3225(2)
c (Å)	17.8937(1)
β (deg)	92.242(2)
V ($Å^3$)	2100.00(4)
Z	4
D_x (Mg/m^3)	1.300

Table 2 FTIR wavenumber assignment for DAST crystal

Wavenumber (cm^{-1})	**Assignment**
3035.96	Vinyl C-H stretch
2914	CH_3 asymmetric stretch
1645.79	C=C stretch/vinyl C-H rocking
1583	C=C symmetric stretch
1551.51	C=C ring stretch
1479.35	CH_3 asymmetric deformation
1527.63, 1435.18 and 1413.47	C=C ring stretch

1369.87	CH_2 bending and C-N stretching
1343.47	CH_3 asymmetric deformation
1320.73	C=C ring stretch
1228.5 and 1210.77	C-H ring stretch
1180.35 and 1165.17	S=O stretch of sulfonate group
1031.43 and 1010.07	Ring C-H stretch
947.96	Vinyl C-H stretch
892	C-N stretch
825.51	1,4-Distribution in the aromatic ring
713.23	Phenyl ring C-H out of plane bending
684.35	Ring CCC
675	The cis-orientation of the substitute at the olefinic double bond
566	CH_3 twisting (Toluene group)
536	Phenyl ring C-H out of plane bending